

PACS numbers: 42.65.Tg; 42.81.Dp
DOI: 10.1070/QE2015v045n09ABEH015690

Generation of a broad IR spectrum and *N*-soliton compression in a longitudinally inhomogeneous dispersion-shifted fibre

I.O. Zolotovskii, D.A. Korobko, O.G. Okhotnikov, D.A. Stolyarov, A.A. Sysolyatin

Abstract. **The propagation of *N*-soliton pulses in an optical fibre with slowly decreasing, shifted anomalous dispersion has been studied experimentally and theoretically. Using a generalised nonlinear Schrödinger equation, we have constructed an adequate numerical model for light propagation in such fibre. Using numerical simulation, we have shown that the use of dispersion-decreasing fibres ensures higher average dispersive radiation intensity and better uniformity of the supercontinuum spectrum. A reduction in the third-order dispersion of such fibres enables supercontinuum generation with a bandwidth exceeding that in homogeneous fibres by several hundred nanometres even in the case of a medium-power subpicosecond source.**

Keywords: *dispersion-shifted fibres, generation of a broad spectrum, longitudinally inhomogeneous optical fibres.*

1. Introduction

One frequently used method of optical pulse compression relies on a nonlinear mechanism of *N*-soliton pulse formation, which operates when a primary pulse propagates in an anomalous-dispersion fibre [1, 2]. Silica dispersion-shifted fibres (DSFs) are of interest for pulse compression in the telecom window ($\lambda \sim 1.56$ μm) because they have low ($\sim$1 ps^2 km^{-1}) anomalous dispersion in this spectral range. Since the square of the soliton order N is inversely proportional to dispersion, $N^2 = \gamma P_0 \tau_0^2/|\beta_2|$ (where β_2 and γ are the group velocity dispersion and nonlinearity coefficients of the fibre, and τ_0 is the initial pulse duration), considerable compression in such fibres is possible for pulses with a comparatively low initial peak power P_0 [1, 3]. The value of τ_0 is determined by the light source and is $\sim$1 ps in the case of standard semiconductor and fibre lasers.

I.O. Zolotovskii, D.A. Korobko Ulyanovsk State University, ul. L. Tolstogo 42, 432017 Ulyanovsk, Russia; e-mail: rafzol.14@mail.ru, korobkotam@rambler.ru;
O.G. Okhotnikov, D.A. Stolyarov Ulyanovsk State University, ul. L. Tolstogo 42, 432017 Ulyanovsk, Russia; present address: Optoelectronics Research Centre, Tampere University of Technology, Korkeakoulunkatu 3, 33101 Tampere, Finland; e-mail: oleg.okhotnikov@tut.fi;
A.A. Sysolyatin A.M. Prokhorov General Physics Institute, Russian Academy of Sciences, ul. Vavilova 38, 119991 Moscow, Russia; Ulyanovsk State University, ul. L. Tolstogo 42, 432017 Ulyanovsk, Russia; e-mail: alexs@fo.gpi.ru

Received 8 October 2014; revision received 22 December 2014
Kvantovaya Elektronika **45** (9) 844–852 (2015)
Translated by O.M. Tsarev

The problem of soliton compression of a pulse in an optical fibre is closely related to the problem of generation of a broad emission spectrum – optical supercontinuum. In the visible and near-IR spectral regions, this problem can be successfully solved by launching a laser pulse of wavelength $\lambda = 600-1000$ nm into a highly nonlinear photonic crystal fibre [4, 5]. In the telecom range, this problem is of particular current importance because of the rapid development of multichannel communication systems [6]. The generation of a broad spectrum in this region can be achieved, for example, using highly nonlinear Ge-doped fibres [7]. At the same time, an important part of the mechanism responsible for the generation of light with a broad spectrum is a resonance energy exchange between a soliton pulse and dispersive waves propagating in the fibre, which takes place near the zero dispersion region [4, 5, 8]. It is for this reason that silica DSFs are potentially attractive for the generation of a broad spectrum in the telecom range [8–10].

In this paper, we report an experimental and theoretical study of the dynamics of a laser pulse in a DSF whose dispersion varies along its length. Among reports concerned with the propagation of light pulses in optical fibres with varying dispersion, of particular interest are those dealing with the generation of parabolic pulses in normal dispersion-decreasing fibres [11, 12], a reduction in frequency modulation of pulses in normal dispersion-increasing fibres [13, 14] and similariton compression of frequency-modulated sech pulses in anomalous dispersion-decreasing fibres [15–17]. In contrast to previous studies [18, 19], which considered adiabatic compression of a fundamental soliton in a fibre with slowly decreasing dispersion, the use of a DSF allows us to examine the propagation of a pulse in the form of a higher order soliton ($N > 1$) in such fibres. This significantly complicates pulse dynamics and enriches the picture of the evolution of its spectrum. The purpose of this work is to study effects that help to improve the quality of broadband generated light and identify optimal compression conditions for a pulse propagating in such fibres.

2. Experiment

The experimental setup used in our studies is schematised in Fig. 1. An input pulse is generated by an erbium-doped all-fibre source with a centre wavelength λ_0 near 1.56 μm. Mode locking is ensured by nonlinear polarisation rotation in the ring cavity of the laser. The output pulse power amplifier comprises a pump diode, wavelength-division multiplexer (WDM) and erbium-doped fibre. An optical isolator is placed

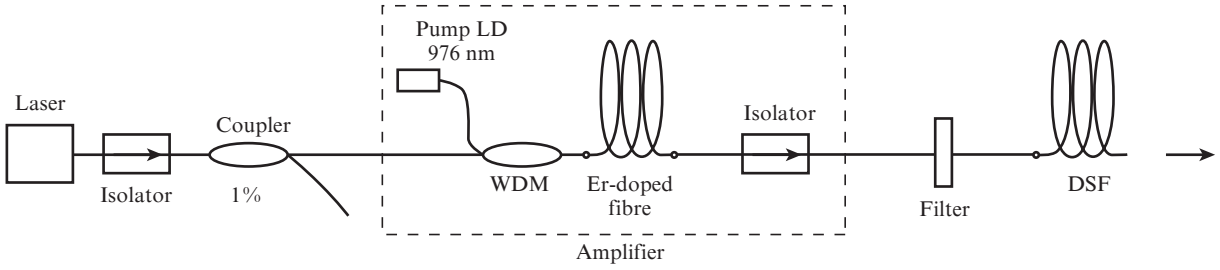

Figure 1. Schematic of the experimental setup.

between the cavity and amplifier. Spontaneous emission and unabsorbed pump light are blocked by a filter at the source output. Pulses are generated at a repetition rate of 80.9 MHz. An autocorrelation analysis indicates that the pulse envelope is sech^2-shaped and that the pulse duration varies from 0.88 to 0.54 ps, depending on gain, which is accompanied by an increase in peak pulse power from 17 to 170 W.

In our studies, we used a 60-m length of an inhomogeneous DSF fabricated at the Fiber Optics Research Center, Russian Academy of Sciences. Its outer diameter decreased monotonically from 86.9 (at the input) to 86.1 μm (at the output). Figure 2 shows the group velocity dispersion (GVD) of the fibre as a function of wavelength for these fibre diameters. It is seen that, at a wavelength $\lambda = 1.56$ μm, the anomalous GVD β_2 decreases from –2.25 to –1.71 ps^2 km^{-1} with decreasing fibre diameter. Along the length of the fibre, β_2 varies exponentially, with an exponent of –4.5 km^{-1}. The third-order dispersion (TOD) parameter is $\beta_3(\omega_0) = 0.11$ ps^3 km^{-1}, and the zero-dispersion wavelength lies in the range 1.530–1.535. The optical loss in the fibre is under 0.3 dB km^{-1}, and the mode field diameter at $\lambda = 1.56$ μm is 6 μm, which corresponds to a nonlinearity coefficient $\gamma \approx 3$ W^{-1} km^{-1}.

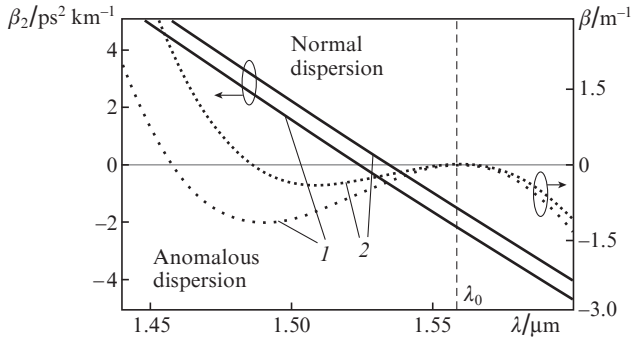

Figure 2. GVD curves of the DSF under study (solid lines) and $\beta = {}^1/_2\beta_2(\omega_0)(\omega - \omega_0)^2 + {}^1/_6\beta_3(\omega_0)(\omega - \omega_0)^3$ dispersion curves relative to the pulse carrier frequency ω_0 corresponding to $\lambda_0 = 1.56$ μm (dotted lines) at fibre diameters of (*1*) 86.9 and (*2*) 86.1 μm.

The fibre was butt-coupled to the source, and its output end was connected to an autocorrelator or spectrum analyser. Figure 3 shows the emission spectrum and autocorrelation traces obtained at the fibre output after a 0.6-ps pulse with a peak power of 132 W had been launched into the fibre. It is seen that, at the DSF output, broadband radiation (30-dB bandwidth above 300 nm) is generated, which consists of a well-defined, high-peak-power individual pulse, a group of low-peak-power pulses and broadband dispersive radiation. This picture is, in principle, consistent with known experimental data on supercontinuum generation in DSFs [8–10]. Figures 4 and 5 show spectral dependences and autocorrelation traces obtained at the output of the inhomogeneous DSF for different pulse durations (τ_0) and peak powers (P_0) at the amplifier output (i.e. at the DSF input). The duration of the well-defined individual pulse with the highest peak power was 0.14–0.15 ps. The maximum power of this peak was estimated at 505, 280 and 95 W, depending on the input pulse power.

It is seen in Fig. 3 that the spectral characteristics and autocorrelation traces measured for pulses propagating in the forward and backward directions in the inhomogeneous fibre differ significantly, i.e. a nonreciprocity effect is observed.

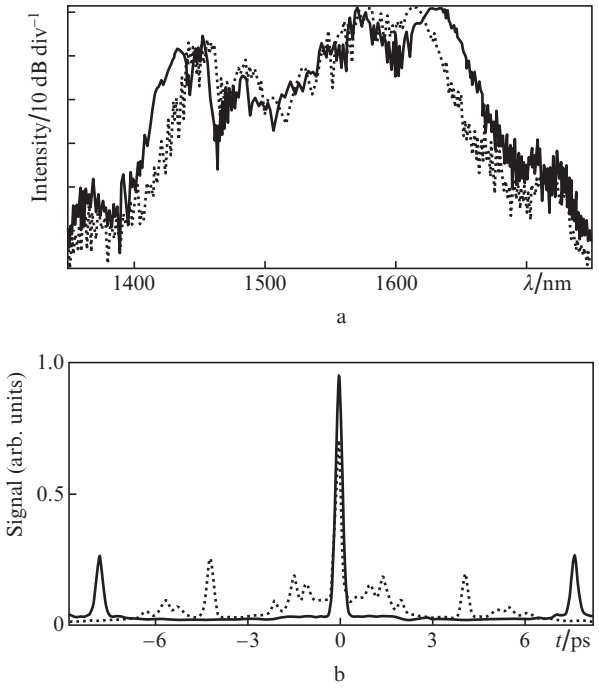

Figure 3. (a) Emission spectra and (b) autocorrelation traces at the output of the inhomogeneous DSF. The solid lines represent a forward pass (decreasing fibre diameter) and the dotted lines represent a backward pass.

3. Model

The propagation of a subpicosecond light pulse with a carrier frequency ω_0 along the longitudinal coordinate z of an inhomogeneous DSF can be described using a generalised non-

linear Schrödinger equation (NLSE) for an $A(z,t)$ complex amplitude [1]:

$$\frac{\partial A}{\partial z} + \frac{i\beta_2(z)}{2}\frac{\partial^2 A}{\partial t^2} - \frac{\beta_3}{6}\frac{\partial^3 A}{\partial t^3} = i\gamma\left(|A|^2 A + \frac{2i}{\omega_0}\frac{\partial}{\partial t}(|A|^2 A) - \tau_R A\frac{\partial |A|^2}{\partial t}\right). \quad (1)$$

Here t is the retarded time; γ is the nonlinearity coefficient; and τ_R is the SRS parameter. We limit the dispersion expansion to the third-order term, assuming that only the GVD $\beta_2(z)$ varies along the length of the fibre.

It can be seen from Fig. 2 in particular that the TOD parameter $\beta_3(\omega_0) = \partial\beta_2/\partial\omega|_{\omega=\omega_0}$ varies insignificantly with fibre diameter. As an illustration, Fig. 2 shows the dispersion curve of the propagation constant of a small-amplitude wave,

$$\beta = {}^1\!/_2\beta_2(\omega_0)(\omega-\omega_0)^2 + {}^1\!/_6\beta_3(\omega_0)(\omega-\omega_0)^3,$$

at the two fibre ends. Note also that a small change in fibre diameter has a negligible effect on the mode area, so the parameter $\gamma(z)$ can be taken to be constant in the model. Absorption can be neglected because it is weak and the fibre is short. Analysis of the spectrum of the primary pulse leads us to think that its frequency modulation is insignificant, so in specifying the initial conditions of the model the input pulse can be represented in the form $A_0(t) = \sqrt{P_0}\,\mathrm{sech}(t/\tau_0)$. Equation (1) was solved numerically using the standard split-step Fourier method [1]. The proposed model allows one to consider a complete picture of the evolution of a propagating pulse. Simulation results are compared to experimental data in Figs 4 and 5. It is seen that there is good agreement. This leads us to conclude that the model adequately describes our experiments.

4. Discussion

Figure 6 presents numerical simulation results which illustrate the variation in the temporal and spectral characteristics of

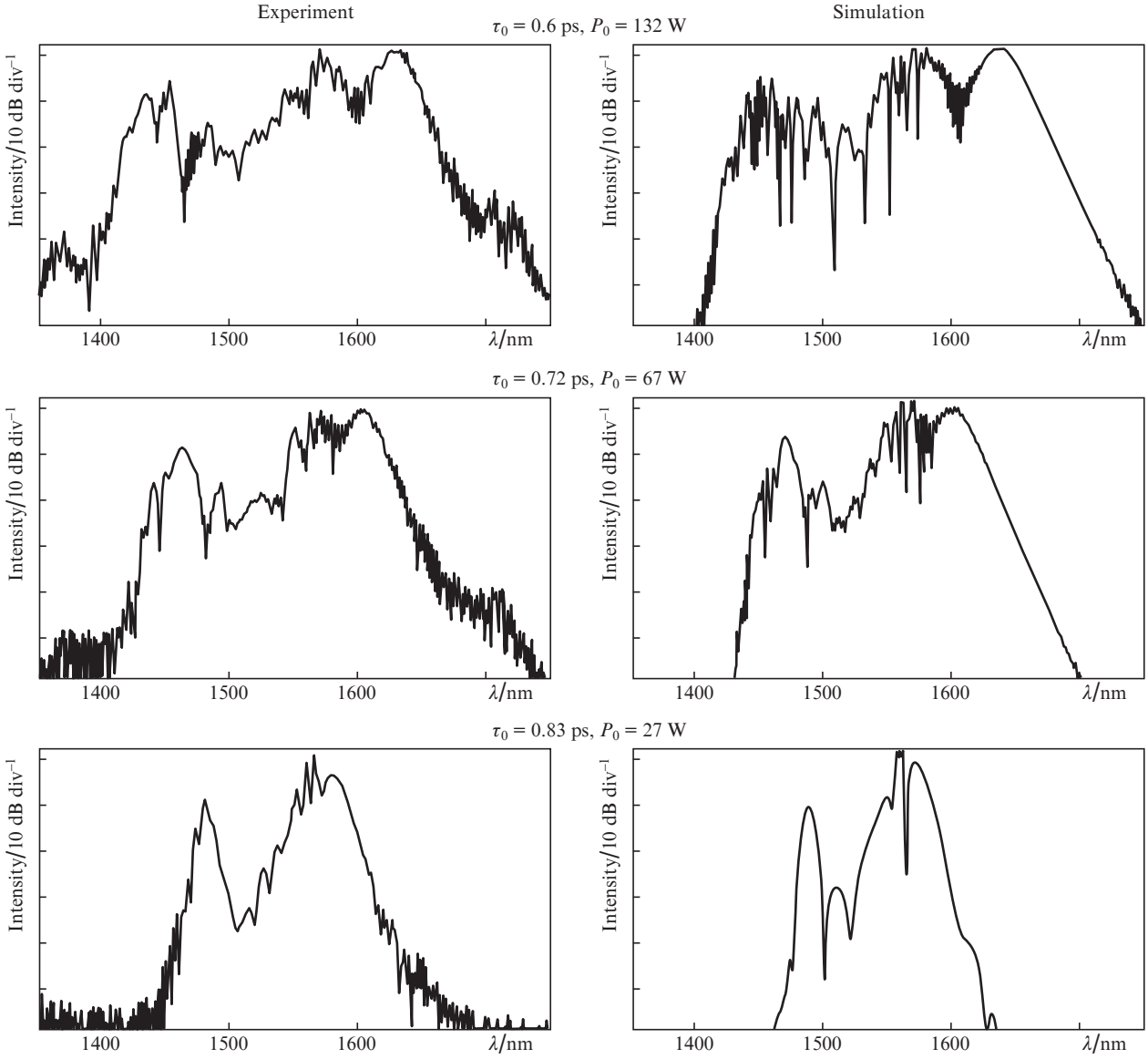

Figure 4. Measured (left) and calculated (right) spectra obtained at the DSF output at different input pulse parameters.

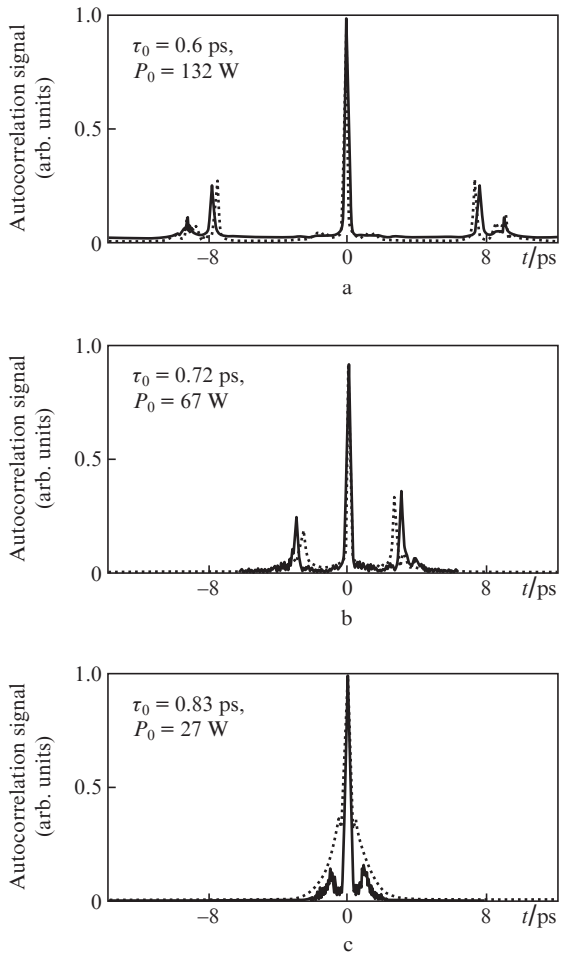

Figure 5. Measured (solid lines) and calculated (dotted lines) autocorrelation traces obtained at the DSF output at different parameters of the pulse launched into the fibre.

light when a primary pulse of duration $\tau_0 = 0.6$ ps and peak power $P_0 = 132$ W propagates through the fibre. Consider the main stages in the evolution of the primary pulse. In the first stage, the pulse experiences compression due to self-phase modulation (SPM) and anomalous dispersion, and its spectrum becomes much broader. In the next stage, the first fundamental soliton separates from the main pulse. Because of the SRS effect, it then propagates separately. In the next stage, the next fundamental soliton separates, etc. This process has been investigated in rather great detail [1, 2, 5, 20]. It is the first stage which is *N*-soliton compression, where a sharp peak emerges on a broad pedestal, instead of the primary pulse. It is reasonable to take that the boundary of the first stage is the instant when the maximum peak power and bandwidth are reached. In the case of constant dispersion [$\beta_2(z) =$ const], the corresponding fibre length (fission length) can be estimated as [5]

$$L_{\text{fiss}} = \frac{L_{\text{d}}}{N} = \frac{\tau_0}{\sqrt{\gamma P_0 |\beta_2|}}, \qquad (2)$$

where L_{d} is the dispersion length. The compression factor of the primary pulse is determined primarily by its order N. Note that the intensity of the broad pedestal in the autocorrelation function also increases with N [2, 21].

Owing to SRS, the separately propagating pulses 'line up' according to their peak power: the pulse that was the first to separate is the shortest and has the highest peak power [1, 20, 22]. For the same reason, the spectrum of each individual pulse shifts to longer wavelengths, and the shift is largest in the case of the pulse with the highest peak power. In a fibre whose dispersion $\beta_2(z)$ decreases along its length, every fundamental soliton experiences adiabatic compression [16, 18, 19]. At the same time, the strong frequency dependence of the dispersion of DSF, $\beta_2(z,\omega) = \beta_2(z,\omega_0) + \beta_3(z,\omega_0)(\omega - \omega_0)$,

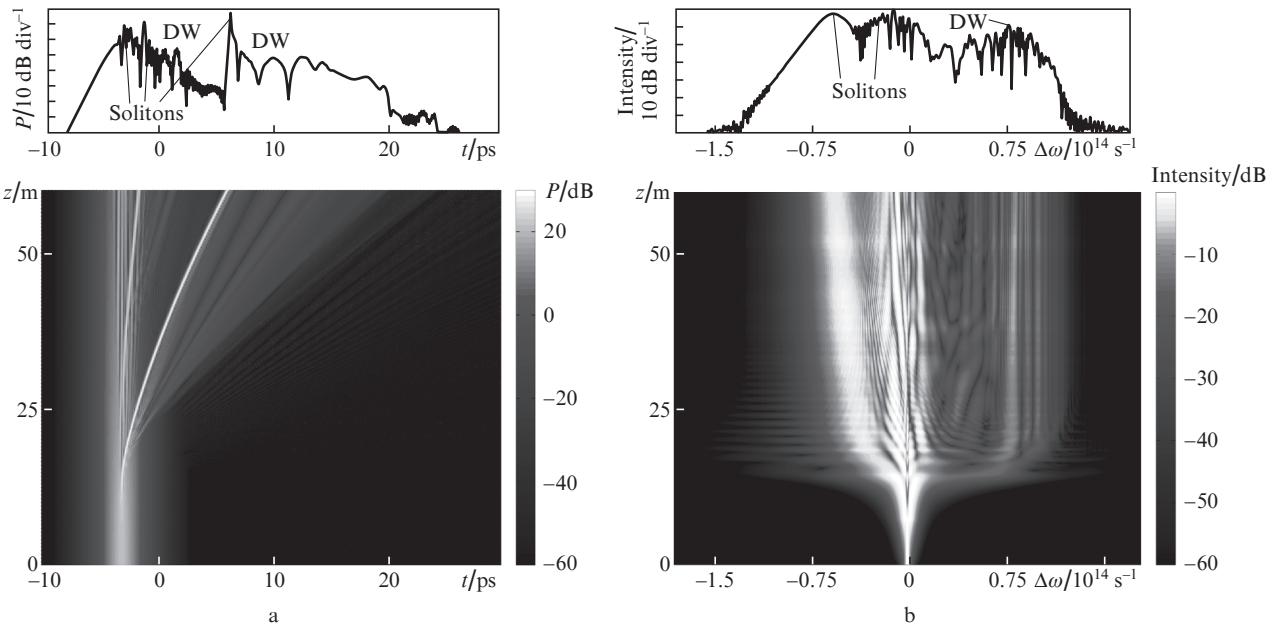

Figure 6. Numerical simulation results: evolution of the (a) temporal envelope and (b) spectrum of a primary pulse ($\tau_0 = 0.6$ ps, $P_0 = 132$ W) propagating through the fibre; DW = dispersive wave.

has important implications. The Raman shift causes the spectrum of the soliton to shift to longer wavelengths and higher anomalous dispersion. As a result, fundamental soliton compression is possible when the rate of the decrease in β_2 along the length of the fibre meets the following condition (where ω_s is the centre wavelength in the spectrum of the soliton) [18]:

$$\left|\frac{\partial\beta_2}{\partial z}\right| > -\beta_3\frac{\partial\omega_s}{\partial z}. \quad (3)$$

If the rate of the decrease in dispersion along the length of the fibre does not meet this condition, the adiabatic adjustment of the soliton to the 'local' anomalous dispersion $\beta_2(z,\omega)$ leads (according to the soliton formula) to an increase in τ and decrease in peak power P: $\tau = 2\beta_2/\gamma W$ and $P = \gamma W/4\beta_2$, where W is the soliton energy.

Figure 7a illustrates the variation in the maximum peak power of light when different primary pulses propagate through the fibre. The pulse orders N_0 were calculated at the initial point at $\beta_2 = -2.25$ ps^2 km^{-1}. The initial pulse duration and peak power correspond to those considered above in analysis of the numerical model. To the maximum compression of the primary pulse there corresponds a region whose coordinates can be found approximately from relation (2). Next, after the pulse fission, the peak power $P(z)$ of the first separated soliton changes. Rapid changes in $P(z)$ are caused by the interaction of the soliton with the rest of the pulse. As the soliton propagates, the oscillation amplitude decreases.

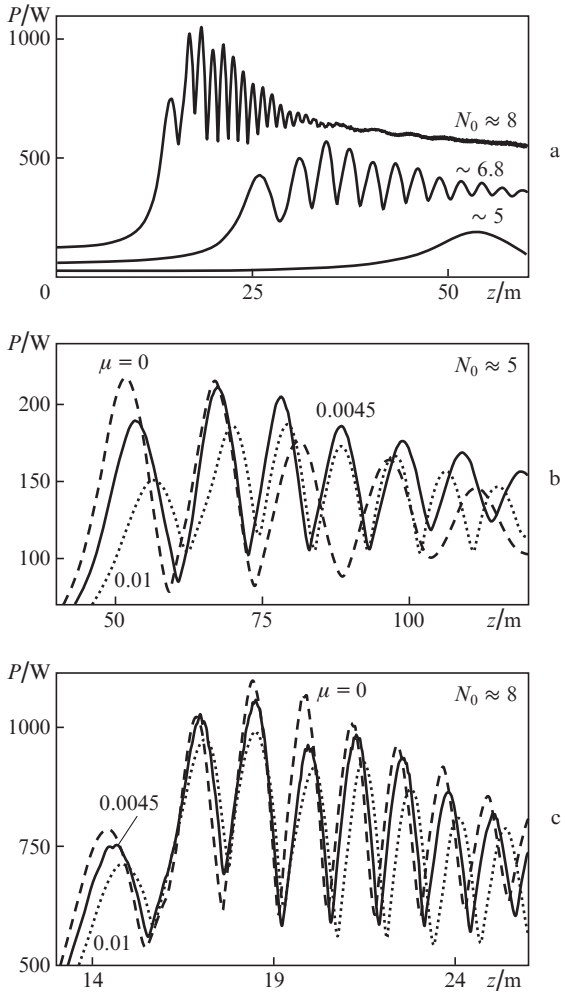

Figure 7. Numerical simulation results: (a) variation in the maximum peak power of different primary pulses [$P_0 = 132$ W, $\tau_0 = 0.6$ ps ($N_0 \approx 8$); $P_0 = 67$ W, $\tau_0 = 0.72$ ps ($N_0 \approx 6.8$); $P_0 = 27$ W, $\tau_0 = 0.83$ ps ($N_0 \approx 5$)] propagating through fibre; (b) variation in the maximum peak power of a primary pulse with $P_0 = 27$ W and $\tau_0 = 0.83$ ps propagating through fibres with different rates of the decrease in dispersion $\beta_2(z)$; (c) same for a pulse with $P_0 = 132$ W and $\tau_0 = 0.6$ ps.

Figures 7b and 7c illustrate how the peak power $P(z)$ varies when a primary pulse propagates in a fibre with constant dispersion and with different rates of the decrease in dispersion along its length: $\beta_2(z) = \beta_2(0)\exp(-\mu z)$. Figure 7b presents results for a primary pulse of lower power ($N_0 \approx 5$). To obtain a complete picture, the simulation was continued to beyond the actual fibre length ($L = 60$ m). It is seen that N-soliton compression occurs earlier in the constant-dispersion fibre, because of the higher local value of β_2, and that the peak power reached in this fibre exceeds that in the dispersion-decreasing fibre. Comparing the variations in peak power in the fibres with different rates of the decrease in $\beta_2(z)$ along their length, we note that adiabatic compression only slightly decreases the rise in dispersion due to the Raman shift. The same applies to Fig. 7c, but at a higher order N of the primary pulse the highly nonlinear N-soliton compression process results in a higher peak with a broader spectrum. The Raman shift has an even faster rate (which strongly depends on the width of the spectrum of the soliton, $\Delta\omega_s$: $d\omega_s/dz \propto \beta_2\Delta\omega_s^2$ [1,20]) and almost completely suppresses the compression induced by the longitudinal decrease in dispersion.

Thus, we are led to conclude that, in the case of pulses with a soliton order $N \geqslant 5$, the use of dispersion-decreasing fibres for N-soliton compression is ineffective. Moreover, at the given $\beta_3 = 0.11$ ps^3 km^{-1}, the next stage in the adiabatic compression of the fundamental soliton is also ineffective. To compress solitons with the peak power obtained, it is necessary to use dispersion-decreasing fibres with reduced TOD (so-called dispersion-flattened fibres) [23,24]. One possible line of future experiments is the use of cascade schemes where N-soliton compression occurs in a constant-dispersion fibre, and subsequent stages are related to adiabatic compression of fundamental solitons in a dispersion-decreasing fibre.

Along with compression, one of the most important effects related to pulse propagation through a fibre is energy transfer to small-amplitude background radiation. This resonance process is usually referred to as dispersive-wave generation. One condition for the generation of a low-power wave at the frequency ω_{DW} is phase matching between the soliton and dispersive radiation: $\beta_s(\omega_{DW}) = \beta_{DW}(\omega_{DW})$, where β_s and β_{DW} are the propagation constants of the soliton and dispersive waves. Neglecting higher order dispersion terms, we obtain the following condition for dispersive-wave generation [4, 25, 26]:

$$\tfrac{1}{2}\beta_2(\omega_0)(\omega_{DW}-\omega_0)^2 + \tfrac{1}{6}\beta_3(\omega_0)(\omega_{DW}-\omega_0)^3 = \beta_{s0} + \beta_{s1}(\omega_s)(\omega_{DW}-\omega_s) + \gamma P/2. \quad (4)$$

The phase matching process is illustrated in Fig. 8. It is seen from Fig. 8a that, in a constant-dispersion fibre, the frequency of dispersive-wave generation by a soliton, ω_{DW} (filled circles 1 and 2), systematically shifts to shorter wavelengths because of the Raman shift of the soliton and the increase

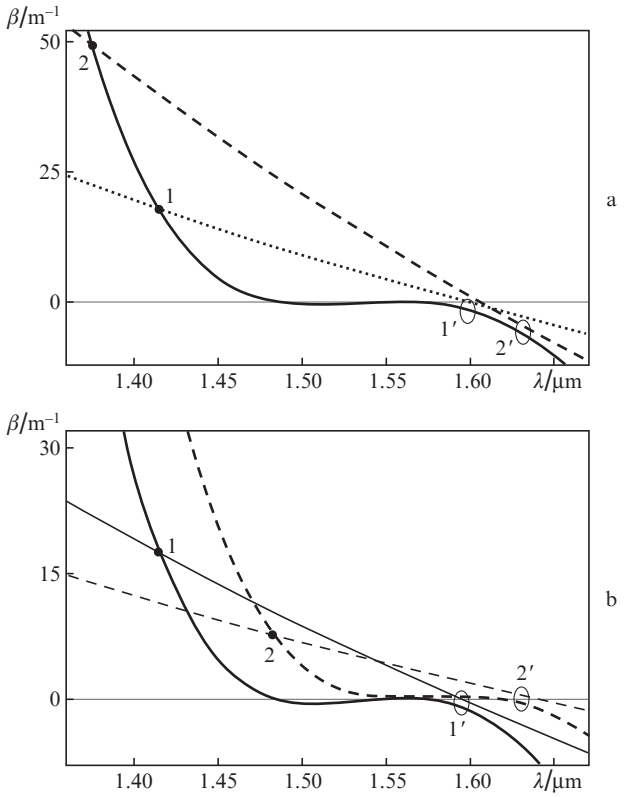

Figure 8. Phase matching for dispersive-wave generation (a) in a constant-dispersion fibre [solid line, $\beta(\omega)$ dispersion curve; dotted and dashed lines, dispersion curves of a soliton pulse, $\beta_s = \beta_{s0} + \beta_{s1}(\omega_s)(\omega - \omega_s) + \gamma P/2$, at points of the fibre with $z_1 < z_2$ and with an increase in the Raman shift of the soliton ($\omega_{s1} > \omega_{s2}$)] and (b) in a fibre with decreasing anomalous GVD [the solid lines correspond to coordinate $z(1')$, and the dashed lines, to coordinate $z(2') > z(1')$; the thick lines represent the dispersion curves of linear waves of resonance radiation and the thin lines represent the dispersion curves of the soliton].

in its group velocity $\beta_{s1}(\omega_s) = \partial\beta/\partial\omega|_{\omega_s}$. It is worth noting in this context that the intensity of the dispersive waves being excited decreases because of the increase in the difference between the centre frequency of the soliton (ω_s) and the generation frequency (ω_{DW}), since the amplitude of the radiation is proportional to $\exp(-a^2|\omega_{DW} - \omega_s|)$, where a = const and $|\omega_{DW} - \omega_s| \propto z$ [25].

In Fig. 8b, this process is examined for two points in a fibre with decreasing dispersion $\beta_2(z)$. States 1′ and 2′ correspond to two points in the fibre [$z(2') > z(1')$], differing in anomalous dispersion [$\beta_2(1') = -2$ ps^2 km^{-1}, $\beta_2(2') = -1.5$ ps^2 km^{-1}], and to an increase in the Raman shift of the generating soliton ($\omega_{s1} > \omega_{s2}$). The decrease in anomalous dispersion as the soliton propagates through the fibre ensures a shift of the zero-dispersion frequency (inflection in the dispersion curve) to longer wavelengths and a shift of the frequency ω_{DW}.

An important distinction from the case of homogeneous fibre is the decrease in the difference $\omega_{DW} - \omega_s$, which is due not only to the shift of ω_{DW} but also to the decrease in the velocity of the soliton, $\beta_{s1}(\omega_s)$. Thus, dispersive radiation in a fibre with decreasing $\beta_2(z)$ should have a more uniform spectrum in comparison with a constant-dispersion fibre, with an increased intensity in the region between the short-wavelength edge of the spectrum and the soliton region (long-wavelength limit). This statement will be verified in what follows using numerical simulation.

Consider the following problem: at particular fibre drawing conditions, i.e. at a given initial GVD, $\beta_{20} = \beta_2(\omega_0)$, and given TOD ($\beta_3$), find the rate of the longitudinal variation in GVD that ensures the most intense dispersive-wave generation without changes in the width of the spectrum. Note that the possibility of primary pulses differing in energy should be taken into account. To solve this problem, we restrict our consideration to fibres with a linear GVD profile: $\beta_{20}(z) = \beta_{20}(1 - \theta z/L)$, where $\theta > 0$ specifies the rate of the decrease in GVD. The above numerical model for pulse propagation remains valid. Critical for its applicability is the variation of the nonlinearity coefficient γ along the length of the fibre, but experimental data indicate that, in the type of fibre in question, the variation in outer diameter, leading to changes in GVD, has a weak effect on the mode area, which determines γ. Upon a change in fibre diameter from 80 to 88 μm, which corresponds to a planned change in GVD at a wavelength $\lambda = 1.56$ μm in the range $\beta_{20} = -2.5$ to 1 ps^2 km^{-1}, the parameter γ changes within 3%, which allows us to neglect changes in it [24].

Let us fix the TOD and initial GVD of the fibre at $\beta_3 = 0.11$ ps^3 km^{-1} and $\beta_{20} = -2.25$ ps^2 km^{-1}, which correspond to the sample studied here. This value of β_{20} seems to be optimal because it allows us to combine the initial GVD value that ensures a high soliton order N with the possibility of a substantial decrease in GVD along the length of the fibre in the anomalous dispersion region. As indicated above, β_3 plays an important role in determining the characteristics of propagating light. The effect of TOD on them will be considered below.

We now turn from a qualitative (Fig. 8) to a quantitative analysis of the characteristics of a supercontinuum generated in different fibres with varying dispersion. Figure 9 shows numerically simulated characteristics of supercontinuum in fibres differing in the rate of the decrease in GVD for two distinct primary pulses. Figures 9a and 9b illustrate the behaviour of the 30-dB bandwidth (within the band in question, the intensity may drop to below this level). Note that, even though the fibres differing in the rate of the decrease in GVD, θ, are rather close in spectral bandwidth, at the given $\beta_3 = 0.11$ ps^3 km^{-1} the supercontinuum in the fibres with lower θ values is broader, which can be accounted for by the slower rate of the shift of the first separated soliton ($d\omega_s/dz \propto |\beta_2|$). Note also that, for broadband generation, the fibre length should exceed the fission length L_{fiss} and that a higher peak pulse power ensures a broader spectrum. This is caused by the large Raman shift of the first separated soliton, with a high peak power and broad spectrum. Recall that the shift rate strongly depends on the bandwidth $\Delta\omega_s$: $d\omega_s/dz \propto \Delta\omega_s^4$. At a lower primary-pulse power, these effects are substantially weaker, and the width of the supercontinuum increases considerably more slowly with fibre length.

The properties of the spectral distribution of supercontinuum can be characterised by the logarithm of the relative intensity (in dB):

$$I(\omega) = 10\lg\left(\frac{|\tilde{A}(\omega)|^2}{\max|\tilde{A}(\omega)|^2}\right) \leqslant 0.$$

The distribution of this random variable provides an idea of the average supercontinuum intensity level. The use of a

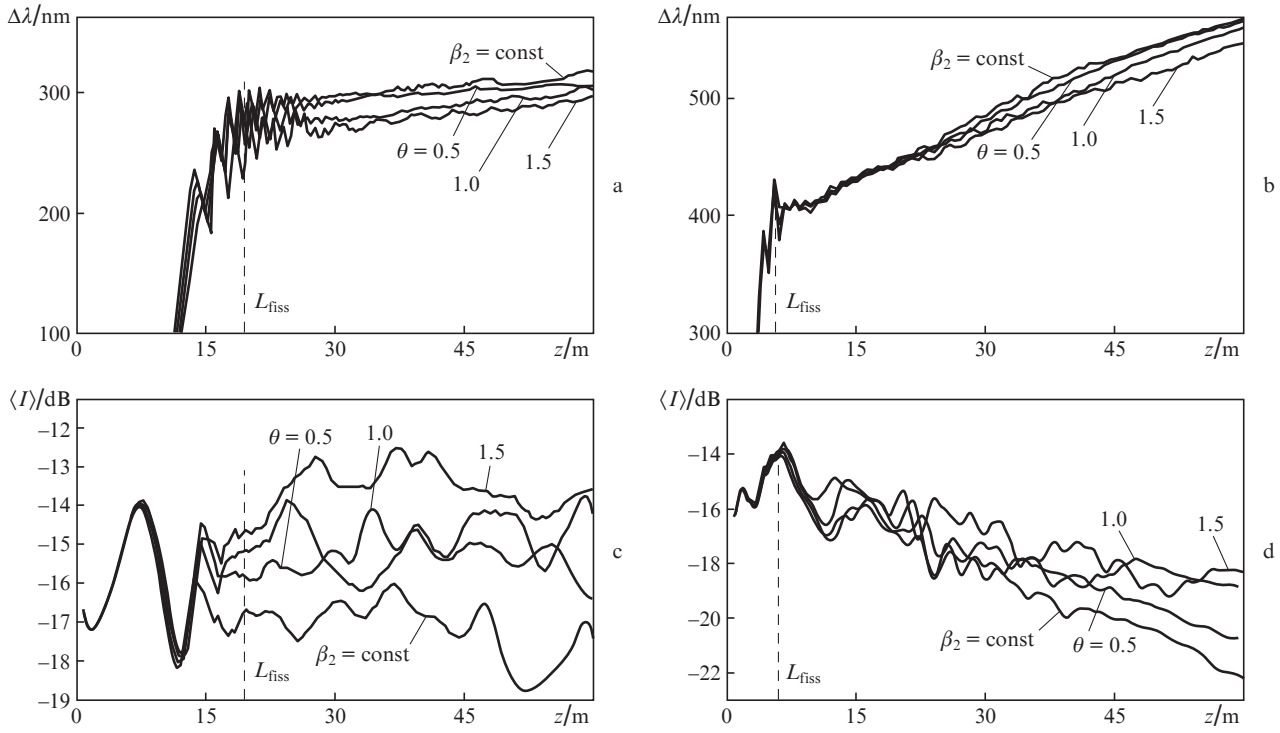

Figure 9. Numerical simulation results: (a, b) 30-dB bandwidth as a function of longitudinal coordinate for the supercontinuum generated in a fibre with decreasing GVD, $\beta_2 = \beta_{20}(1 - \theta z/L)$ ($L = 60$ m); (c, d) average logarithm of the intensity within the band in question. Primary-pulse parameters: (a, b) $\tau_0 = 0.6$ ps, $P_0 = 132$ W; (c, d) $\tau_0 = 0.3$ ps, $P_0 = 528$ W.

logarithmic scale allows us to estimate the intensity of dispersive radiation, which levels off in the presence of soliton pulses when the relative intensity $|\tilde{A}(\omega)|^2/\max|\tilde{A}(\omega)|^2$ is considered. Figures 9c and 9d show the longitudinal variation of the average logarithm of the intensity,

$$\langle I\rangle = \frac{1}{\omega_2-\omega_1}\int_{\omega_1}^{\omega_2} I(\omega)\,\mathrm{d}\omega = \frac{1}{\omega_2-\omega_1}\sum_{\omega_1}^{\omega_2} I(\omega_k)\,\Delta\omega_k, \qquad (5)$$

within the band in question. Points ω_2 and ω_1 are the rightmost and leftmost points of the spectrum, where the condition $I(\omega) = -30$ dB is met. Note that, for clarity of illustration, fast fluctuations were averaged.

The following trend was found in the variation of $\langle I\rangle$ with z: the emergence of a new resonance band in the spectrum corresponds to a region where $\langle I\rangle$ increases. Moreover, the change $\Delta\langle I\rangle$ is proportional to $I(\omega_k)$, related to a new resonance band at a frequency ω_k. Regions of growth alternate with those where $\langle I\rangle$ falls off, which is due to both the periodic variation in the characteristics of the soliton and the overall broadening of the averaging range $\Delta\lambda$. It is seen from Fig. 9d for $\theta \leqslant 1$ that the termination of the generation of resonance bands by the first separated soliton and stabilisation of its parameters lead to an asymptotically smooth decrease in $\langle I\rangle$ with increasing z, which is determined by the increase in $\Delta\lambda$. In Figs 9c and 9d, no asymptotics can be identified at $\theta = 1.5$, but the observed results lead us to the following important conclusion: since dispersion-decreasing fibres have a larger number of dispersive radiation bands (Fig. 8), which have higher average intensity (Fig. 9), the supercontinuum generated in such fibres has a more uniform structure, which is of paramount importance for most applications.

Even more significant results on supercontinuum generation can be obtained by solving the problem of TOD management in silica DSFs whose GVD varies along their length. As mentioned above, known approaches to this problem take advantage of dispersion-flattened fibres [23, 24].

Figure 10a presents the characteristics of supercontinuum in fibres with different β_3 values at a particular rate of the decrease in GVD along the fibre length: $\theta = 1$. As TOD decreases to 0.04 ps^3 km^{-1}, we observe the generation of a rather uniform supercontinuum more than 500 nm in width. Note that the right part of Fig. 10a demonstrates broadening of the spectrum of the first separated fundamental soliton, accompanied by a decrease in β_3, i.e. a reduction in its duration and an increase in its peak power. This means that the above-mentioned mechanism of adiabatic soliton compression is effective in fibres with low β_3. The increase in the width of the spectrum of the first and subsequently separated solitons as they propagate through the fibre leads to the generation of new resonance emission bands, improves the uniformity of the supercontinuum and increases its width.

Figure 10b shows the 30-dB bandwidth of the supercontinuum vs. TOD for fibres differing in the rate of the decrease in GVD. At low β_3, the difference between the soliton frequency (ω_s) and the frequency of generated waves (ω_{DW}) increases, reducing the efficiency of dispersive-wave generation. In the case of a homogeneous fibre, the intensity of dispersive waves is so low that they fall within the 30-dB bandwidth only for $\beta_3 > 0.035$ ps^3 km^{-1}. This shows up as a characteristic step in the $\beta_2 = \text{const}$ curve. Nevertheless, efficient compression of a separated soliton in fibres with

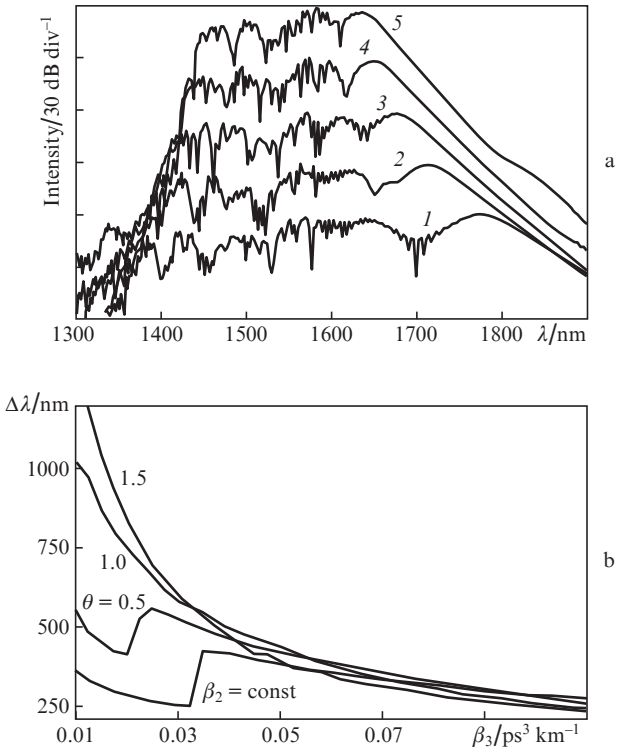

Figure 10. Numerical simulation results: (a) spectra obtained at the output of fibres of length $L = 60$ m with decreasing GVD, $\beta_2 = \beta_{20}(1 - \theta z)$, $\theta = 1$, for a primary pulse with $\tau_0 = 0.6$ ps and $P_0 = 132$ W at $\beta_3 =$ (*1*) 0.04, (*2*) 0.06, (*3*) 0.08, (*4*) 0.1 and (*5*) 0.12 ps^3 km^{-1}; (b) 30-dB bandwidth as a function of TOD for the supercontinuum generated in a fibre of length $L = 40$ m with varying GVD: $\beta_2 = \beta_{20}(1 - \theta z/L)$.

a large decrease in GVD ($\theta > 1$) offers the possibility of generating broad resonance emission bands even at a large $\omega_{DW} - \omega_s$ frequency difference. It can be seen that the 30-dB bandwidth of the supercontinuum in dispersion-decreasing fibres then exceeds that in homogeneous fibres by several hundred nanometres. With increasing TOD, the solitonic and dispersive parts of the spectrum approach each other, restoring the picture observed in Figs 9a and 9b: the spectra of longitudinally inhomogeneous and constant-GVD fibres are close in width. Thus, we conclude that TOD minimisation in dispersion-decreasing fibres ensures a considerable increase in the efficiency of supercontinuum generation in such fibres.

5. Conclusions

The propagation of *N*-soliton pulses in fibres with slowly decreasing, shifted anomalous dispersion has been studied experimentally and theoretically. It has been shown experimentally that, when subpicosecond pulses with a peak power corresponding to a soliton order $N \approx 8$ are launched into a fibre, the output emission spectrum has a 30-dB bandwidth near 320 nm. Analysis of pulses propagating in the forward and backward directions has revealed a nonreciprocity effect: narrowing of the spectrum and reduction in the peak power of the main emission peak when the pulse propagates through the fibre in the backward direction.

Using a generalised NLSE, we have constructed an adequate numerical model for light propagation in the fibre studied. *N*-soliton compression and dispersive radiation generation in the type of fibre in question have been studied by numerical simulation. The simulation results suggest that a considerable variation in GVD along the fibre length is necessary for raising the dispersive radiation intensity in such fibres. In particular, for the linear profile $\beta_{20}(z) = \beta_{20}(0)(1 - \theta z/L)$ ($\beta_{20} \sim -2.5$ ps^2 km^{-1}) the reduction parameter should be $\theta \geqslant 1$ at fibre lengths $L \sim 30$ m and above. The most ambitious results can be obtained through the drawing of fibres with decreasing flattened GVD. Adiabatic soliton compression ensures considerable supercontinuum broadening, whereas the average intensity and the high uniformity of the spectrum remain unchanged. Simulation results indicate that, with TOD reduced to a level of 0.03–0.04 ps^3 km^{-1}, a medium-power source can ensure a supercontinuum bandwidth above 700 nm in the telecom range, which is extremely attractive for the development of demultiplexing systems. The present results will be used in formulating design specifications for the fabrication of inhomogeneous fibres for experiments on optical supercontinuum generation in the telecom range.

Acknowledgements. This work was supported by the RF Ministry of Education and Science (state research task, Project No. 14.Z50.31.0015). A.A. Sysolyatin received support from the Russian Foundation for Basic Research (Grant No. 14-02-00856).

References

1. Agrawal G. *Nonlinear Fiber Optics* (Burlington: Academic Press, 2007).
2. Mollenauer L., Tomlinson W., Stolen R., Gordon J. *Opt. Lett.*, **8**, 289 (1983).
3. Wai P.K.A., Menyuk C.R., Chen H.H., Lee Y.C. *Opt. Lett.*, **13**, 628 (1987).
4. Zheltikov A.M. *Usp. Fiz. Nauk*, **176**, 623 (2006).
5. Dudley J.M., Genty G., Coen S. *Rev. Mod. Phys.*, **78**, 1135 (2006).
6. Morioka T., Mori K., Saruwatari M. *Electron. Lett.*, **29**, 862 (1993).
7. Okuno T., Onishi M., Kashiwada T., Ishikawa S., Nishimura M. *IEEE J. Sel. Top. Quantum Electron.*, **5**, 1385 (1999).
8. Hori T., Nishizawa N., Goto T., Yoshida M. *J. Opt. Soc. Am. B*, **21**, 1969 (2004).
9. Gu Y., Zhan L., Deng D.D., Wang Y.X., Xia Y.X. *Laser Phys.*, **20**, 1459 (2010).
10. Moon S., Kim D. *Opt. Express*, **14**, 270 (2006).
11. Hirooka T., Nakazava M. *Opt. Lett.*, **29** (5), 498 (2004).
12. Finot C., Barviau B., Millot G., Guryanov A., Sysoliatin A., Wabnitz S. *Opt. Express*, **15** (24), 15824 (2007).
13. Korobko D., Okhotnikov O., Sysolyatin A., Yavtushenko M., Zolotovskii I. *J. Opt. Soc. Am. B*, **30**, 582 (2013).
14. Zolotovskii I.O., Korobko D.A., Sementsov D.I. *Phys. Wave Phenomena*, **21**, 110 (2013).
15. Kruglov V.I., Peacock A.C., Harvey J.D. *Phys. Rev. E*, **71**, 056619 (2005).
16. Korobko D., Okhotnikov O., Zolotovskii I. *J. Opt. Soc. Am. B*, **30**, 2377 (2013).
17. Zolotovskii I.O., Korobko D.A., Okhotnikov O.G., Sysolyatin A.A., Fotiadi A.A. *Kvantovaya Elektron.*, **42**, 828 (2012) [*Quantum Electron.*, **42**, 828 (2012)].
18. Chernikov S.V., Mamyshev P.V. *J. Opt. Soc. Am. B*, **8**, 1633 (1991).
19. Chernikov S., Richardson D., Payne D., Dianov E. *Opt. Lett.*, **18**, 476 (1993).
20. Tai K., Bekki N., Hasegawa A. *Opt. Lett.*, **13** (5), 392 (1988).
21. Dianov E.M., Mamyshev P.V., Prokhorov A.M. *Kvantovaya Elektron.*, **15**, 5 (1988) [*Sov. J. Quantum Electron.*, **18**, 1 (1988)].

22. Kutz J., Lynge C., Eggleton B. *Opt. Express*, **13**, 3989 (2005).
23. Tamura K.R., Nakazawa M. *IEEE Photonics Technol. Lett.*, **11**, 319 (1999).
24. Akhmetshin U.G., Bogatyrev V.A., Senatorov A.K., Sysolyatin A.A., Shalygin M.G. *Kvantovaya Elektron.*, **33**, 265 (2003) [*Quantum Electron.*, **33**, 265 (2003)].
25. Skryabin D.V., Luan F., Knight J.C., Russell P.S. *Science*, **301**, 1705 (2003).
26. Skryabin D.V., Gorbach A.V. In: *Supercontinuum Generation in Optical Fibers* (Cambridge: Cambridge Univ. Press, 2010) p. 178.